Entropy optimization of a FENE-P viscoelastic model: a numerically guided comprehensive analysis

Razi Khan[1] · Eugenia Rossi di Schio[2] · Paolo Valdiserri[2]

Abstract

The influence of polymers on entropy generation processes is substantial, particularly in the fields of fluid dynamics and rheology. The FENE-P (Finitely Extensible Nonlinear Elastic-Peterlin) model describes the polymer's dynamics as a result of the interaction between the stretching caused by the velocity gradient and the elastic force that restores the polymer to its equilibrium position. Models such as FENE-P aid in understanding and predicting polymer flow behaviour allowing for the reduction of entropy generation by optimizing system designs. A continuum approach is employed to express the heat flux vector and polymer confirmation tensor of the model. The study investigates the complex relationship between polymer conformation, flow dynamics, and heat transfer taking into account the thermophoresis (Soret effect) and mass diffusion-thermal diffusion coupling (Dufour effect) phenomena to optimize processes by reducing entropy. This study illuminates polymer's significance in entropy minimization, improving engineering design methodologies and applications in materials science, chemical engineering, and fluid dynamics. As result, the presence of polymers leads to a substantial decrease in the total entropy of the system. This understanding provides opportunities for enhancing heat transfer systems, thereby facilitating the development of more efficient and sustainable technology.

Keywords Entropy generation · Polymers · FENE-P model · Soret and Dufour effects · Bejan number · Numerical solution · Similarity solution

Abbreviations

b	Extensibility parameter	Du	Dufour number
Be	Bejan number	h_f	Convective heat transfer ($Wm^{-2}K^{-1}$)
Bi	Biot number	k	Thermal conductivity ($Wm^{-1}K^{-1}$)
Br	Brinkmann number	$\tilde{k}$	Mean absorption coefficient
C	Solute concentration of fluid (kgm^{-3})	L	Diffusive variable
c_p	Specific heat at constant pressure ($m^2s^{-2}K^{-1}$)	$\widetilde{L}$	Characteristics length (m)
C_w	Solute concentration at wall (kgm^{-3})	N_g	Entropy generation number
C_∞	Ambient solute concentration of fluid (kgm^{-3})	Nr	Thermal radiation parameter
D_m	Mass diffusivity coefficient (m^2s^{-1})	Nur	Reduced Nusselt number
D_T	Thermal diffusion ratio (m^2s^{-1})	Pr	Prandtl number
		Re	Reynolds number
		Sc	Shmidth number
		Sf	Drag force/skin friction coefficient
		Shr	Reduced Sherwood number
		Sr	Soret number
		T	Dimensional temperature (K)
		T_m	Mean fluid temperature (K)
		T_w	Wall temperature (K)
		T_∞	Ambient fluid temperature(K)
		$U(x)$	Stretching velocity (ms^{-1})
		u, v	Velocity components (ms^{-1})
		u_o	Dimensional constant ($L^{2/3}T^{-1}$)

✉ Eugenia Rossi di Schio
eugenia.rossidischio@unibo.it

Razi Khan
razi.khan@unicampania.it

Paolo Valdiserri
paolo.valdiserri@unibo.it

1 Department of Mathematics and Physics, University of Campania, "Luigi Vanvitelli", Caserta 81100, Italy

2 Department of Industrial Engineering, University of Bologna, Bologna, Italy

W_i	Weissenberge number
α_1	Temperature difference parameter
α_2	Concentration difference parameter
β	Retardation parameter
γ	Fluid relaxation time (s)
μ	Dynamic viscosity ($kgm^{-1}s^{-1}$)
ν	Polymers kinematic viscosity (m^2s^{-1})
ρ	Density (kgm^{-3})
σ	Thermal diffusivity (m^2s^{-1})
$\widetilde{\sigma}$	Stefan-Boltzmann constant

Introduction

Analysing and reducing entropy generation are effective approaches for improving or maximizing the thermodynamic efficiency of engineering systems. The imperative to construct and operate efficient systems has consistently shown to be a powerful driving force for the technological advancement. In light of the evident scarcity of resources in the present day, the significance of efficiency and resource preservation has grown significantly in recent times. Thus, second law of thermodynamics methods for analysing and improving engineering systems are popular. Entropy is a key metric used in fluid mechanics to analyse irreversible mass and heat transport. Irreversibility is the primary factor contributing to the rise in entropy. Over the years, several numerical and theoretical research have focused on entropy generating approaches to anticipate and examine the durability of mechanical or electrical components. The usefulness of fluid mechanics in engineering and industrial processes is crucial for the design and construction of heat transfer devices such as coolers and evaporators. Research from experimental studies verifies that increased entropy generation has a detrimental impact on the efficiency of engineering technology. The crucial function of entropy generation in minimizing the need for extra energy sources in a system is generally well acknowledged. In order to improve efficiency and performance in a variety of technical and commercial applications, including electrical and motor control, switches, temperature sensors for power conversion, and so forth, the researcher's main objective is to decrease entropy generation.

In physics, entropy generation is defined as a rise in the overall entropy of a system and its surrounding. In simple words, it is a measure of a system's disorder or unpredictability. In this regard, Bejan [1–3] pioneered the concept of entropy generation minimization by applying basic thermodynamic laws and heat transfer processes of fluid mechanics. It is essential to analyse the factors that contribute to the production of entropy in order to advance technology, reduce energy waste, and increase efficiency in accordance with the fundamental laws of thermodynamics. Indeed, to increase

the heat transfer nanofluids have been introduced [4–7] to take advantage of the Brownian diffusion and thermophoresis. The usual nanofluid comprises a single nanoparticle. In the past few years, attention on heat transfer in hybrid nanofluids and in biofluids has been paid by the scientific literature due to its proficiency to intensify heat conduction rate than the usual nanofluid, and due to the possible interesting applications in many technological fields [8–10]. Among them, useful applications are in semiconductors, solar cells, transistors, tissue engineering, electronic circuits, drug delivery, biosensing, integrated circuit baseboards, cosmetic fillers, plastics, paint, tape, rubber, grinding belts, catalyst carriers, aerospace aircraft, and more. Concerning entropy generation, Asad et al. [11] studied the entropy generation in a magnetohydrodynamic (MHD) Prandtl fluid. They considered the Soret and Dufour effects and an unsteady stretched surface. Non-linear mixed convection and convective conditions for surface heat and mass transfer were also investigated. Patel et al. [12] explored the generation of entropy in a vertical channel using Casson nanofluid, specifically focusing on the Soret and Dofour effects. Khan et al. [13] studied the entropic effects of Darcy-Forchheimer MHD radiative flow together with Soret and Dufour effects. Sami et al. [10] conducted a study on Carreau MHD mathematical model to describe the generation of entropy across a curved stretched surface, taking into account the Soret and Dufour effects. In their investigation, Ibrahim et al. [14] examined the generation of entropy in an incompressible, continuous bioconvection flow. The research investigation incorporated the Soret and Dufour effects, in addition to the impact of the magnetic field. The research conducted in [15] examined the entropy generation of a tri-hybrid nanofluid flow with electromagnetic properties in a porous medium governed by Darcy-Forchheimer equations. The flow occurred across a stretched sheet under convective conditions. A Reiner-Rivlin fluid's hydrodynamic flow around a stretched cylinder was studied by Hayat et al. [16]. The effects of convective conditions, the Soret effect, and the Dufour effect were all taken into account in the study. Fluid flow on a heated rotating disc employing Bingham plastic fluid was the subject of the numerical analysis in the study [17]. Considering the effect of entropy generation, the study also highlighted the thermo-physical properties and energy dissipation as a result of viscous dissipation. For more detail studies on entropy generation, the articles [18–23] describe some of the significant and noteworthy investigations.

Continuum approaches are frequently used in the practical application of numerical simulations for turbulent flows containing polymer solutions. A time-varying tensor field is used to describe the polymer conformation in this technique. An example of a tensor field in this case is the polymer conformation tensor, which shows the average inertia tensor of polymers at certain points and periods in the fluid. We

need to take into consideration the average of a non-linear function connected to the end-to-end vector of the polymer across temperature fluctuations in order to derive an evolution equation for the provided conformation tensor from the FENE dumbbell model. A mean-field closure approach was proposed by Peterlin [24] to tackle this difficulty. Using the force value at the mean-squared polymer extension instead of averaging the elastic force across temperature changes yields the FENE-P model [25]. Within the FENE-P model framework, a stress tensor field that depends on the polymer conformation tensor characterises the interaction between polymers and the flow. Turbulent fluxes in polymer solutions may be accurately modelled using this continuum model. This procedure requires solving the Navier–Stokes equation with an elastic-stress factor and the polymer conformation tensor at the same time. Numerical simulations focusing on reducing turbulent drag thus make heavy use of the FENE-P model. Because of the model's asymptotic behaviour for high shear rates, a significant Newtonian viscosity is not required to maintain stable fluid behaviour. The model works very well for a wide range of shear rates with just one relaxing time. This model basically works on the basis of limited extensibility. In this model, the polymeric liquid rheological constitutive equations also show a polymer chain as a dumbbell with two beads linked by a spring. The beads are small molecules of different monomers, and the spring is the entropic effects on the polymer's end-to-end vector.

In the literature, the use of polymeric nanofluids to enhance the heat transfer has been investigated delving deeper into the possible technological applications [26]. Concerning the possible flow models, indeed, in the recent literature most of the focus in the last 20 years has been on the viscoelastic flow properties and heat transfer of the FENE-P model. For example Olagunju [27, 28] and Cortell [29] have studied the steady two dimensional boundary layer flow using the FENE-P constitutive equation. Olagunju [30] and Anabtawi and Khuri [31] on the other hand discussed the generalized viscoelastic Falkner-Skan flow governed by FENE-P model. Airal et al. [32] looked at how the FENE-P model behaved when it moved over a magnetically stretched surface. Khan et al. looked into how the FENE-P model moved and transferred heat when nanoparticles and microorganisms were present [33]. Recently, analyses concerning how the FENE-P model responded were presented, investigating when it was driven past a Riga plate under strong suction [34] and when polymers and dust particles were present [35]. Further interesting studies on the FENE-P model are the publications [36–39] and the references cited therein.

The primary impetus and originality of the present investigation lie in:

- Exploring the significance of polymers additives as entropy generation reducing agents;

- Considering the role of nanofluids altering entropy generation and reducing irreversibility;
- Utilizing the influences of Soret and Dufour effects as entropy minimization strategies;
- Aiming to contribute to the development of efficient entropy minimization strategies using the FENE-P model in engineering and commercial applications.

In this paper, section "Mathematical formulation" includes the mathematical interpretation of the model followed by similarity transformation and quantities of physical interest. Entropy generation analysis is covered in section "Entropy generation optimization", while method of solution is briefly explained in section "Solution method". In section "Numerical comparison and code validation" we present code validation and a numerical comparison of the existing problem with the already published results. The last two sections "Results and discussion" and "Conclusion" are devoted to the results discussion and key findings of the present article.

Mathematical formulation

We suppose a steady and two dimensional FENE-P nanofluid flow in the region $y \geq 0$ that is being driven by a semi-infinite horizontal permeable stretching surface and the stretching velocity $U(x)$ varies non-linearly as shown in Fig. 1. Additionally, the temperature T and the nanoparticle volume fraction ϕ are constant at the sheet as indicated by T_w and ϕ_w. The symbols T_∞ and ϕ_∞ indicate the ambient values of T and ϕ. The governing equations that characterize this problem can be represented as follows [27, 40]:
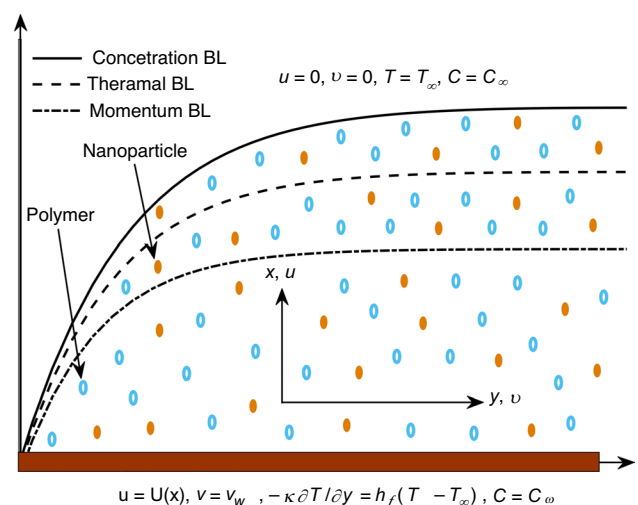
$$\nabla \cdot \widetilde{\mathbf{u}} = 0 \tag{1}$$

Fig. 1 Geometrical representation

$$\rho(\widetilde{\mathbf{u}} \cdot \nabla)\widetilde{\mathbf{u}} = -\nabla P + (\nabla \cdot \widetilde{\mathcal{T}}) \tag{2}$$

where the stress tensor $\widetilde{\mathcal{T}}$ represent the contribution of both the polymers and solvents terms. In his analysis Olagunju [30] derived this relationship in more detail as follows:

$$\widetilde{\mathcal{T}} = \mathcal{T}_s + \mathcal{T}_p = \eta_s\Theta + \mathcal{T}_p, \tag{3}$$

Here, we employ the FENE-P model to show how the polymeric stress tensor, denoted as $\mathcal{T}_p$, and the contribution from the solvent term, denoted as $\mathcal{T}_s$, are correlated according to the Newtonian law $\eta_s\Theta$. The symbol Θ represents the rate of strain tensor in this context. It is defined as the sum of two functions: the transpose of the gradient of $\widetilde{\mathbf{u}}$ and the gradient of the velocity field $\widetilde{\mathbf{u}}$. Additionally, the variable η_s is used to describe the solvent's viscosity. The suggested model represents the polymer as a system of two beads linked by a non-linear spring. The mathematical expression for the constitutive polymeric stress tensor is as follows:

$$\mathcal{T}_p = \frac{\eta_p}{\gamma}Z^{-1}E - I, \;\; Z = 1 - \frac{trE}{b}. \tag{4}$$

In this expression, the term $(\eta_p/\gamma)Z^{-1}E$ represent the material's viscous behaviour under the influence of polymer viscosity (η_p), the fluid relaxation time (γ), and the relaxation state (Z) when subjected to the impact of deformation E. The parameter b represents the ratio between maximum and equilibrium spring lengths, showing polymer extensibility. In order to fulfil the above equation, the conformation tensor E must adhere to specific requirements as follows:

$$(1 - trE)^{-1}E + \gamma E_{(1)} = I, \tag{5}$$

where $tr\,E$ indicates the trace of matrix E, and I represents the identity matrix. The upper convected derivative $E_{(1)}$ may be expressed as:

$$E_{(1)} = \frac{DE}{Dt} - (\nabla\widetilde{\mathbf{u}})^{\mathrm{T}}E - E\nabla\widetilde{\mathbf{u}}, \tag{6}$$

along with the energy equation:

$$(\widetilde{\mathbf{u}} \cdot \nabla)T = \sigma\nabla^2 T - \frac{1}{\rho c_p}\nabla q_r + \frac{D_m D_T}{c_s c_p}\nabla^2 C, \tag{7}$$

and the concentration equation:

$$(\widetilde{\mathbf{u}} \cdot \nabla)C = D_m\nabla^2 C + \frac{D_m D_T}{T_m}\nabla^2 T, \tag{8}$$

where $\nabla u = \partial u/\partial y$ and $\nabla q_r = \partial q_r/\partial y$. We can write the system of Eqs. (1)-(2) and (7)-(8) in standard notation as follows, using the assumed conditions and the Boussinesq and boundary layer approximations:

$$\frac{\partial u}{\partial x} + \frac{\partial v}{\partial y} = 0, \tag{9}$$

$$u\frac{\partial u}{\partial x} + v\frac{\partial u}{\partial y} = \nu\frac{\partial}{\partial y}\left[(1 - \beta + \beta Z)\frac{\partial u}{\partial y}\right], \tag{10}$$

where Z satisfies

$$\kappa\left(\frac{\partial u}{\partial y}\right)^2 Z^3 + Z - \omega = 0, \tag{11}$$

$$u\frac{\partial T}{\partial x} + v\frac{\partial T}{\partial y} = \sigma\frac{\partial^2 T}{\partial y^2} - \frac{1}{\rho c_p}\frac{\partial q_r}{\partial y} + \frac{D_m D_T}{c_s c_p}\frac{\partial^2 C}{\partial y^2}, \tag{12}$$

$$u\frac{\partial C}{\partial x} + v\frac{\partial C}{\partial y} = D_m\frac{\partial^2 C}{\partial y^2} + \frac{D_m D_T}{T_m}\frac{\partial^2 T}{\partial y^2}, \tag{13}$$

the associated boundary conditions are as:

$$\begin{cases} u = U(x), v = v_w(x), \\ -k\frac{\partial T}{\partial y} = h_f(T_w - T_\infty), C = C_w(x) & \text{at} \;\; y = 0, \\ u \to 0, T \to T_\infty, C \to C_\infty & \text{when} \;\; y \to \infty. \end{cases} \tag{14}$$

Here, the velocity components in the x and y directions are represented by $\widetilde{\mathbf{u}} = (u, v)$, ρ represent density in the kinematics viscosity expression $\nu = (\eta_s + \eta_p)/\rho$, the thermal conductivity is represented by σ and the retardation parameter is given by $\beta = \eta_p/(\eta_s + \eta_p)$. Furthermore, $\kappa = 2\gamma^2/(3 + b)$, and $\omega = b/(3 + b)$ where b is the extensibility parameter. The solute's wall concentration is C_w, and C_∞ is the solute's concentration away from the sheet. D_m stands for mass diffusivity coefficient, k for thermal conductivity, h_f for convective heat transfer coefficient, T_m for mean fluid temperature, D_T for thermal diffusion ratio, c_s for concentration susceptibility, and c_p for specific heat at constant pressure.

At the surface ($y = 0$), the conditions shown in Eq. (14) pertain to the direct interactions between the fluid and the surface. These interactions include the velocity resulting from surface movement, the heat flux resulting from convective heat transfer, and the concentration of nanoparticles. Away from the surface (when $y \to \infty$), the conditions guarantee that the fluid properties revert back to their original values, indicating a state where the impact of the surface is insignificant. These conditions jointly define a practical physical phenomena that is applicable to various engineering applications including the movement of fluids, transfer of heat, and transfer of mass.

By considering the Rosseland approximation for radiative heat flux in Eq. (4) in an optically thick fluid utilized in [29], we have the simplified radiative heat flux as:

$$q_{\mathrm{r}} = -\frac{4\widetilde{\sigma}}{3\widetilde{k}}\frac{\partial T^4}{\partial y}, \tag{15}$$

In Eq. (15), the Stefan-Boltzmann constant is represented by $\widetilde{\sigma}$ and the mean absorption coefficient by $\widetilde{k}$. By expressing the term T^4 in Eq. (15) as a linear function of temperature, it is assumed that temperature differences within the flow can be approximated in this manner. Consequently, by expanding T^4 in a taylor series around the free stream temperature T_∞ and neglecting higher-order terms, the obtained expression is:

$$T^4 = 4T_\infty^3 T - 3T_\infty^4 \tag{16}$$

We may convert the non-linear system of governing equations into a set of non-linear similar form by incorporating similarity transformations with the help of stream functions $u = \partial\psi/\partial y, v = -\partial\psi/\partial x$, and the following transformation [40, 41]:

$$U(x) = u_0 x^{1/3}, \quad \eta = y\sqrt{\frac{U(x)}{\nu x}}, \quad \psi = \sqrt{U(x)\nu x}f(\eta),$$
$$Z = g(\eta),$$

$$\theta(\eta)) = \frac{T - T_\infty}{T_{\mathrm{w}} - T_\infty}, \quad \phi(\eta) = \frac{C - C_\infty}{C_{\mathrm{w}} - C_\infty}. \tag{17}$$

Upon employing these transformations, Eq. (9) is identically satisfied, and the resulting Eqs. (10) and (11) reduces to:

$$(1 - \beta + \beta g)f''' + \left(\frac{2}{3}f + \beta g'\right)f'' - \frac{1}{3}f'^2 = 0, \tag{18}$$

$$K_0 g^3 f''^2 + g - \omega = 0, \quad Z = g, \tag{19}$$

where the parameter $K_0 = 2\epsilon/(3 + b), \epsilon = u_0^3 \gamma^2/\nu\widetilde{L} = W_{\mathrm{i}}^2 Re$, $W_{\mathrm{i}} = u_0\gamma/\widetilde{L}$, and $Re = u_0\widetilde{L}/\nu$. Here, W_{i} denotes Weissenberg number, i.e. an elasticity measure of the fluid, while the Reynolds number is represented by Re, with u_0 the dimensional constant and $\widetilde{L}$ the characteristic length. Now, computing g' from Eq. (19) and substituting into Eq. (18) we obtain:

$$\left(1 - \beta + \beta g - \frac{2\beta K_0 f''^2 g^3}{1 + 3K_0 f''^2 g^2}\right)f''' + \frac{2}{3}ff'' - \frac{1}{3}f'^2 = 0, \tag{20}$$

Eq. (20) reduces to Newtonian fluid for $\epsilon = \beta = 0$. For an Oldroyd-B fluid $b \to \infty$, and from Eq. (19) we have $g = \omega = 1$. In other words $K_0 = 0$ and $\omega = 1$, and we get the Blasius equation. Now using Eq. (17) and solving for Eqs. (13) and (14) we get:

$$\left(1 + \frac{4}{3}Nr\right)\theta'' + \frac{2}{3}Prf\theta' + DuPr\phi'' = 0, \tag{21}$$

$$\phi'' + \frac{2}{3}f\phi' + ScSr\theta'' = 0. \tag{22}$$

If the mass transfer rate is chosen as $v_{\mathrm{w}}(x) = -\frac{2}{3}s\sqrt{\frac{U(x)\nu}{x}}$, then the modified boundary conditions become:

$$\begin{cases} f(\eta) = s, f'(\eta) = 1, \theta'(\eta) = -Bi(1 - \theta), \phi(\eta) = 1 & \text{at} \quad \eta = 0, \\ f'(\eta) \to 0, \theta(\eta) \to 0, \phi(\eta) \to 0 & \text{when} \quad \eta \to \infty. \end{cases} \tag{23}$$

where $s = -v_{\mathrm{w}}(x)$ and negative values of s corresponds to blowing while positive values correspond to suction. Here, the Dufour number is represented by $Du = \frac{D_{\mathrm{m}}D_{\mathrm{T}}\Delta C}{C_{\mathrm{s}}c_{\mathrm{p}}\nu\Delta T}$, Soret number by $Sr = \frac{D_{\mathrm{m}}D_{\mathrm{T}}\Delta T}{T_{\mathrm{m}}\nu\Delta C}$, Schmidt number by $Sc = \frac{\nu}{D_{\mathrm{m}}}$, Prandtl number by $Pr = \frac{\nu\rho c_{\mathrm{p}}}{\sigma}$, and thermal radiation parameter by $Nr = \frac{4\widetilde{\sigma}T_\infty^3}{\widetilde{k}\sigma}$. Also, $Bi = \frac{h_{\mathrm{f}}}{k\sqrt{\frac{U(x)\nu}{x}}}$ represents the Biot number. Based on industry observation, the primary significant parameters of interest are the drag force coefficient, reduced Nusselt number, and reduced Sherwood number. These measurements may be expressed using the following expressions:

$$Cf = \frac{\tau_{\mathrm{w}}}{\rho U_{\mathrm{w}}^2}, Nu = \frac{q_{\mathrm{w}}x}{k(T_{\mathrm{w}} - T_\infty)}, Sh = \frac{q_{\mathrm{m}}x}{D_{\mathrm{B}}(C_{\mathrm{w}} - C_\infty)}, \tag{24}$$

where the mass flux q_{m}, heat flux q_{w}, and shear stress flux τ_{w} at the surface have the following formulas:

$$\mu(1 - \beta + \beta Z)\frac{\partial u}{\partial y}\Big|_{y=0} = \tau_{\mathrm{w}}, -k\left(1 + \frac{16\widetilde{\sigma}T_\infty^3}{3\widetilde{k}\sigma}\right)\frac{\partial T}{\partial y}\Big|_{y=0}$$
$$= q_{\mathrm{w}}, -D_{\mathrm{B}}\frac{\partial\phi}{\partial y}\Big|_{y=0} = q_{\mathrm{m}}. \tag{25}$$

Using the similarity transformation and putting Eq. (25) into Eq. (24) we have:

$$\begin{cases} Sf = \sqrt{Re_{\mathrm{x}}}Cf = (1 - \beta + \beta g)f''(0), \\ Nur = \frac{Nu}{\sqrt{Re_{\mathrm{x}}}} = -\left(1 + \frac{4}{3}Nr\right)\theta', \\ Shr = \frac{Sh}{\sqrt{Re_{\mathrm{x}}}} = -\phi', \end{cases} \tag{26}$$

Entropy generation optimization

The degree of irreversibility in a system for a particular process is expressed by entropy generation. The local entropy generation rate L_{G} for a viscous fluid has the following volumetric value:

$$L_{\mathrm{G}} = \frac{\sigma}{T_\infty^2}\left(1 + \frac{16\widetilde{\sigma}T_\infty^3}{3\widetilde{k}\sigma}\right)\left(\frac{\partial T}{\partial y}\right)^2 + \frac{\mu}{T_\infty}(1 - \beta + \beta Z)\left(\frac{\partial u}{\partial y}\right)^2$$
$$+ \frac{RD_{\mathrm{m}}}{T_\infty}\left(\frac{\partial T}{\partial y}\frac{\partial C}{\partial y}\right) + \frac{RD_{\mathrm{m}}}{C_\infty}\left(\frac{\partial C}{\partial y}\right)^2.$$

$$(27)$$

In the current flow problem involving fluid friction and heat transfer, Eq. (27) elucidates the main source of irreversibility. The specified entropy generation rate, denoted as $\widetilde{S_{\mathrm{G}}}$, provides the optimal levels of entropy generation at which the system achieves thermodynamic optimization. The ratio of L_{G} to $\widetilde{S_{\mathrm{G}}}$, also known as the dimensionless entropy generation number N_{g}, can be written as follows:

$$N_{\mathrm{g}} = \frac{L_{\mathrm{G}}}{\widetilde{S_{\mathrm{G}}}} \tag{28}$$

where,

$$\widetilde{S_{\mathrm{G}}} = \frac{\sigma(\Delta T)^2}{T_\infty^2\left(\frac{y}{\eta}\right)^2}. \tag{29}$$

Putting Eq. (27) and Eq. (29) in Eq. (28), we get

$$N_{\mathrm{g}} = \left(1 + \frac{4Nr}{3}\right)\theta'^2 + \frac{Br}{\alpha_1}(1 - \beta + \beta g)f''^2 + \frac{L}{\alpha_1}\theta'\phi'$$
$$+ \frac{L\alpha_2^2}{\alpha_1^2}\phi'^2. \tag{30}$$

where the temperature difference parameter is represented by $\alpha_1 = \frac{\Delta T}{T_\infty}$, and $\alpha_2 = \frac{\Delta C}{C_\infty}$, is the concentration difference parameter, $Br = \frac{\mu U_{\mathrm{w}}^2(x)}{\sigma \Delta T}$, and $L = \frac{RD_{\mathrm{m}}\Delta C}{\sigma}$, represents diffusive variable. The Bejan number is calculated as follows:

$$Be = \frac{\left(1 + \frac{4Nr}{3}\right)\theta'^2}{\left(1 + \frac{4Nr}{3}\right)\theta'^2 + \frac{Br}{\alpha_1}(1 - \beta + \beta g)f''^2 + \frac{L}{\alpha_1}\theta'\phi' + \frac{L\alpha_2^2}{\alpha_1^2}\phi'^2} \tag{31}$$

According to Eq. (31), the Bejan number lies between zero and one. If Be is much smaller than $0.5\,(Be \ll 0.5)$, the irreversibility of heat transfer is primarily influenced by the entropy generation rate caused by friction irreversibility. Conversely, when Be is much larger than $0.5\,(Be \gg 0.5)$, entropy generation due to irreversible heat transfer prevails over irreversible friction. When Be equals $0.5\,(Be = 0.5)$, the irreversibility of heat transmission and friction are equally significant.

Solution method

We numerically solve the updated system (20)-(23) along with (30) and (31) using the MATLAB programme bvp6c [42], which is based on a finite difference technique. This package is an extension of the bvp4c package [43] and has a sixth-order accuracy. Throughout the integration interval, this collocation formula produces a solution that is accurate up to the sixth order and preserves C^1 continuity. The bvp6c solver employs the residual control structure of bvp4c, with adjustments to enhance the precision of the finite difference approximation. This feature guarantees a degree of accuracy defined by the user and is equally resilient compared to the existing bvp4c method. Furthermore, it attains the necessary precision with a reduced number of internal mesh points and assessments. Consequently, the goal of bvp6c is to efficiently handle the same class of problems while maintaining the precision and resilience of the original bvp4c solver. Throughout the whole computation time, the method, like bvp4c, guarantees constant and predefined correctness. To achieve this goal, the MIRK6 (mono-implicit Runge–Kutta) method [44] is adjusted using the sixth-order interpolant described in [45]. Throughout the whole computational interval, this procedure represents the solution. The polynomial employed in this context satisfies the criteria of collocation, boundary conditions, and continuity at the endpoints of each subinterval. The bvp4c technique may be regarded as a collocation method that utilises a piecewise cubic polynomial function to precisely depict the data acquired via a three-point Lobatto IIIA approximation. Like bvp4c, bvp6c operates on the core idea that both error estimates and mesh selection are dependent on the residual. In addition, due to the fact that these solvers specifically handle first-order differential equations, we transformed the third and second order differential equations into first-order differential equations. By using $\eta_\infty = 7$, we obtained the asymptotic approximations as dictated by boundary conditions (23). The criterion for absolute convergence was established at 1×10^{-7}. To summarise, the MATLAB bvp6c code utilizes a finite difference technique to efficiently and accurately solve complex systems in science and engineering. It achieves this by numerically solving non-linear coupled equations and boundary conditions. By employing this numerical method, we may gain a deeper understanding of the dynamics of systems that cannot be solved analytically.

Numerical comparison and code validation

Given the absence of an exact solution [46, 47] for a nonlinearly stretching boundary problem, it is necessary to solve the system of equations numerically via iterative schemes. To validate and compare the numerical results with the data that has previously been published in the literature, we employ two different methods. Initially, we use the bvp4c and bvp6c Matlab packages to solve the problem. In the second phase, we generalize our problem by taking into account the limiting cases in the absence of a strong suction condition for the numerical results of the wall's velocity gradient and for a large extensibility parameter, in which case the problem simplifies to Oldroyd-B fluid. When no analytical solution is present, the computed solution's error can be assessed by applying a fixed mesh evaluation to the problem and interpolating the numerical solution results at these points (interpolation errors) [42]. Since the solver's accuracy is the key issue, rather than the solution obtained by interpolation of these points, the primary attention is on errors at individual locations. Based on the data in table 1 it is evident that the sixth-order solution is significantly more efficient. This may be attributed to the significantly lower number of mesh points needed to achieve the desired level of accuracy. Additionally, it is possible to make observations on the precision of the solvers. The term error here refers to the difference between the interpolated outcomes obtained by the two solvers. In order to maintain consistency, it is presumed that the intended solution is contained within the initial dimension of f. It is to be noted that bvp6c yields similar results as bvp4c when a smaller tolerance is used, but it computes more precise solutions significantly faster and with a substantially reduced number of mesh points. The plots in Fig. 2 demonstrate that the solution obtained via the bvp6c approach is similar to that obtained through the bvp4c method. Furthermore, the graphs shows how the mesh points for both approaches have a tendency to gather at regions where the solution experiences rapid changes. Taking into consideration these factors, we are confidence that the numerical technique that we are using is, in fact, producing the correct solution. Both approaches provide results that are comparable when just a moderate level of precision is required; however, when this level of precision is raised, bvp6c solves the problem with a significantly less number of mesh points in a less amount of time.

In order to compare our results with the previously published ones, we make a modification to our problem. We examine the general stretching sheet velocity, denoted as $u_w(x) = u_0 x^N$, and follow the same technique as we did for the stretching velocity of the form $u_w(x) = u_0 x^{1/3}$. As a consequence, Eq. (20) is simplified to:

Table 1 Comparison between the two bvpc solvers

bvp4c solution				bvp6c solution			
tol	time	mesh	maxres	time	mesh	maxres	error
$1e^{-3}$	0.4835	50	$9.099e^{-4}$	0.2412	51	$1.526e^{-6}$	$2.450e^{-3}$
$1e^{-6}$	0.1356	116	$8.012e^{-7}$	0.1265	132	$6.604e^{-9}$	$8.634e^{-9}$
$1e^{-7}$	0.0971	163	$9.897e^{-8}$	0.0640	147	$6.599e^{-9}$	$3.269e^{-9}$
$1e^{-8}$	0.0814	320	$9.172e^{-9}$	0.0619	148	$2.379e^{-9}$	$4.571e^{-10}$
$1e^{-9}$	0.1592	614	$9.882e^{-9}$	0.0948	98	$8.174e^{-10}$	$6.288e^{-11}$
$1e^{-10}$	0.5894	1105	$9.940e^{-11}$	0.1648	142	$7.566e^{-11}$	$3.596e^{-12}$

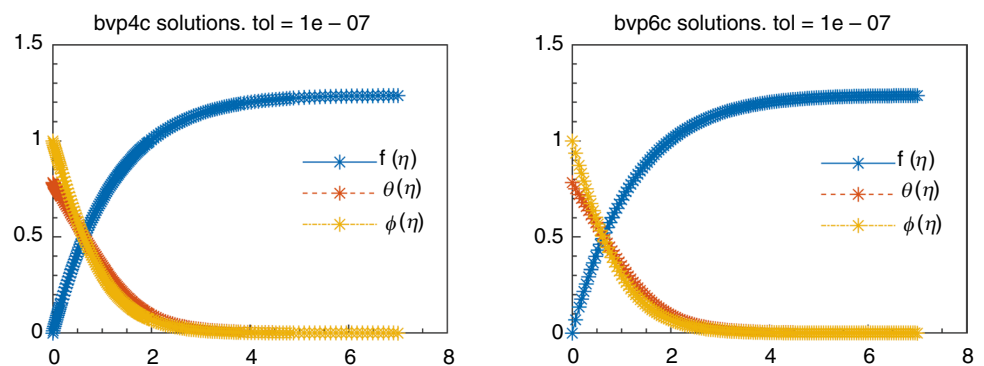**Fig. 2** The FENE-P solution plots generated by bvp4c and bvp6c

Table 2 Numerical results of the wall's velocity gradient when $s = 0$ and $b \to \infty$

N	$-f''(0)$ in Ref. [46]	$-f''(0)$ in Ref. [48]	$-f''(0)$ in current paper
0.0	0.6275	0.6283	0.6278
0.2	0.7667	0.7675	0.7671
0.5	0.8894	0.8901	0.8897
1.0	1.0000	1.0005	1.0001
3.0	0.1485	1.1490	1.1487
10.0	1.2348	1.2352	1.2350
20.0	1.2574	1.2578	1.2576

$$\left(1 - \beta + \beta g - \frac{2\beta K_0 f''^2 g^3}{1 + 3K_0 f''^2 g^2}\right) f''' + ff'' - \frac{2N}{N+1} f'^2 = 0,$$

(32)

The provided numerical results presented in table 2 demonstrates that our findings and the numerical results correlate well with the previously reported data in [46, 48].

Results and discussion

Some quantities of physical interest like drag force, Nusselt number, and Sherwood number have already discussed in detail in the literature [33, 34]. Hence, in this paper we mainly focus to analyse the impact of fluid flow parameters, such as $(0.5 \leq \beta \leq 1.5)$, $(5 \leq b \leq 30)$, $(\epsilon = 0.3)$, $(Nr = 1)$, $(s = 3)$, $(Pr = 7)$, $(0.1 \leq Du \leq 0.3)$, $(0.05 \leq Sr \leq 0.3)$, $(3 \leq Sc \leq 5)$, $(2 \leq Bi \leq 5)$, $(3 \leq Br \leq 5)$, $(0.25 \leq \alpha_1 \leq 0.5)$, $(0.25 \leq \alpha_2 \leq 0.75)$, and $(1 \leq L \leq 3)$, on entropy generation, Bejan number, as well as the role of polymers in reducing entropy. The FENE-P model incorporates the retardation parameter, which refers to the capacity of the polymer chain to unwind and turn back to its equilibrium configuration. An increase in the retardation parameter results in a prolonged relaxation of the polymer chains, which subsequently impacts the rheological properties of the fluid

and, consequently, the generation of entropy. As the retardation parameter increases, the relaxation of the polymer chains is prolonged, resulting in a deceleration of the fluid's response to deformation. As a consequence, the total dissipative processes and viscous dissipation within the fluid both reduces as a result of this behaviour. Entropy generation is frequently linked to irreversibility and dissipation; therefore, a reduced rate of polymer chain relaxation leads to reduced entropy generation, as shown in Fig. 3a. The generation of friction-related entropy reduces with the increase in retardation parameter as shown in Fig. 3b, when the Bejan number is below 0.5. This observation reinforces the significance of polymer chain relaxation in determining the irreversibility of fluid flow and offers legitimacy to the notion that fluid motion, and more specifically friction, is the primary contributor to entropy generation within the system. The extensibility parameter is essential for characterising the rheological properties of polymeric fluids. As the extensibility parameter increases, the ability of polymer chains to stretch further increases. This has a direct influence on the behaviour of the fluid, resulting in more fluid deformation, improved dissipative processes, and longer relaxation periods. These elements contribute to an increased development of entropy in the system. Furthermore, when the value of b approaches infinity, the model simplifies to Falkner-Skan model. Bhatnagar et al. [49] present the scenario of a viscoelastic effect incorporated into the Newtonian case as a correction of higher-order ($O(Re)$). Consequently, the entropy experiences a substantial rise, as shown in Fig. 4a. Now, let's see how an increase in the extensibility results in a corresponding increase in the Bejan number. Figure 4b demonstrates that when the extensibility parameter expands, the dominance of fluid flow irreversibility becomes more pronounced. The enhanced extensibility enables more deformation of polymer chains, resulting in an increased irreversibilities in fluid flow and, subsequently, a rise in the Bejan number. A decrease in the Dufour number signifies a reduction in the relative significance of mass transfer effects in comparison to heat transfer effects. Therefore, a reduction in the Dufour number indicates a change in the prevailing

Fig. 3 The impact of retardation parameter on N_g and Be
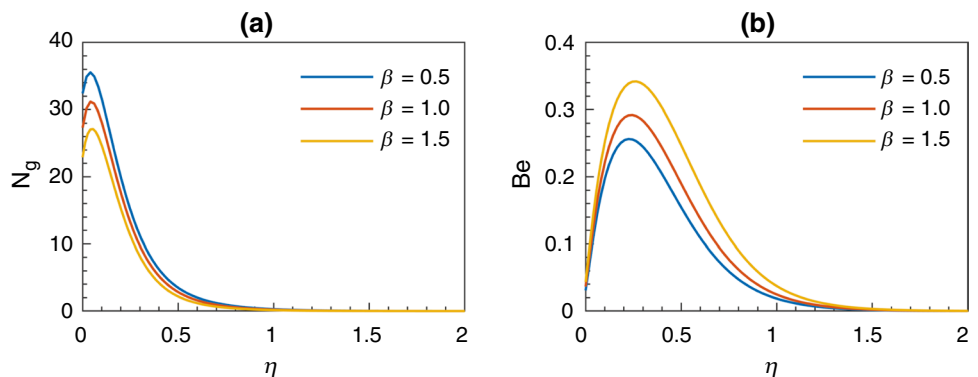
influence of heat transfer compared to mass transfer in the system. As a result, entropy generation is predominantly driven by irreversibilities in heat transport, and lowering the Dufour number reduces total entropy generation in the fluid system under consideration, as shown in Fig. 5a. Furthermore, Fig. 5b demonstrates that a reduction in the Dufour number strengthens the presence of fluid flow irreversibility. The diminished significance of mass transfer corresponds to the pre-existing conditions, resulting in an overall reduction in the Bejan number. The influence of thermal diffusion on mass transfer processes increases as the Soret number increases. The transition from molecular diffusion to thermal diffusion results in enhanced mass transfer efficiency accompanied by diminished irreversibilities. Consequently,

the total number of entropy generated is decreased, primarily due to the diminished entropy generation associated with mass transfer. This phenomenon is shown in Fig. 6a. Similarly, an increase in the Soret number reinforces the dominance of irreversibility in fluid flow, as shown in Fig. 6b. Consistent with the pre-existing conditions, the decreased entropy generation in mass transfer processes as a result of the increased dominance of thermal diffusion causes the Bejan number to decrease overall. We will now examine how the Schmidt number influences the generation of entropy in Fig. 7a. The transition from momentum diffusivity to mass diffusivity occurs when the Schmidt number decreases in fluid flow. As a consequence, the generation of entropy related to friction is reduced, leading to a broad reduction in

Fig. 4 The impact of extensibility parameter on N_g and Be
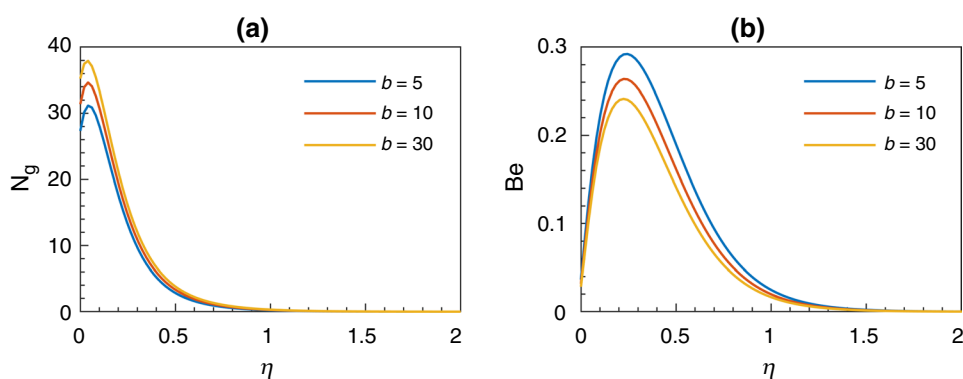
Fig. 5 The impact of Dufour number on N_g and Be
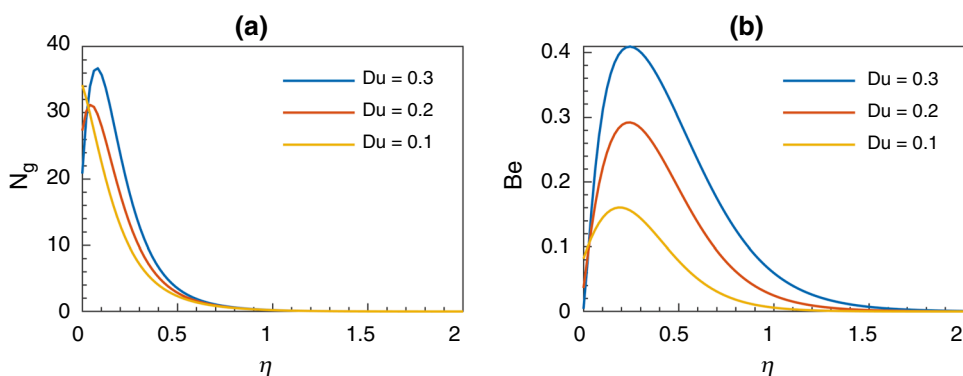
Fig. 6 The impact of Soret number on N_g and Be
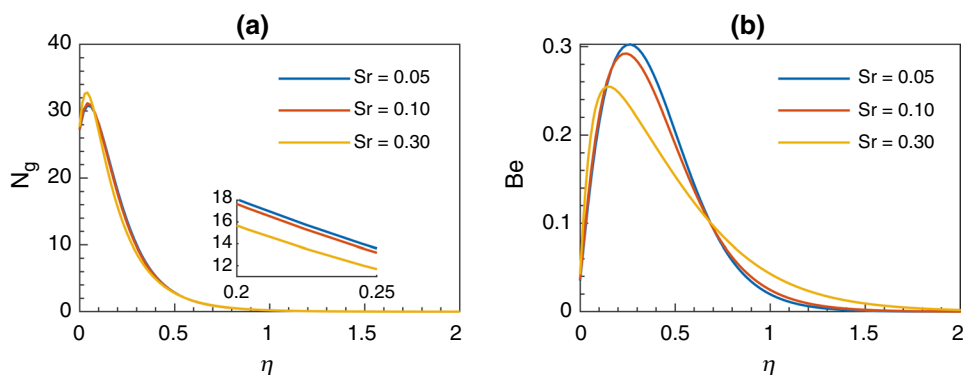
the generation of entropy due to the increased significance of irreversibilities in mass transfer. It is noteworthy to mention, as shown in Fig. 7b, that while the Bejan number remains below 0.5 the reduction in the Schmidt number may enable the Bejan number to approach greater values. Nevertheless, there continues to be a general tendency towards a decline in the irreversibilities of fluid flow and a reduction in the Bejan number. The influence of the Biot number, as shown in Fig. 8a, will now be examined. It is evident that internal heat transmission becomes more efficient in comparison to external heat transfer as the Biot number decreases. As a consequence, there is a decline in the overall irreversibilities of heat transfer and an equivalent reduction in the generation of entropy linked to heat transfer mechanisms occurring

within the solid body. Let us now examine how the Biot number influences the Bejan number. As shown in Fig. 8b, a reduction in the Biot number leads to a corresponding enhancement in the efficacy of internal heat transfer taking place within the solid. Consequently, this leads to a decrease in the overall irreversibilities of heat transfer. Nonetheless, this doesn't affect the dominant role of irreversibility in fluid flow as it pertains to the Bejan number, which ultimately decreases.

As shown in Fig. 9a, the significance of viscous dissipation diminishes in comparison to heat conduction as the Brinkman number decreases. As a consequence, the overall generation of entropy decreases, as the system enhances its thermal efficiency through increased reliance on heat

Fig. 7 The impact of Schmidt on N_g and Be
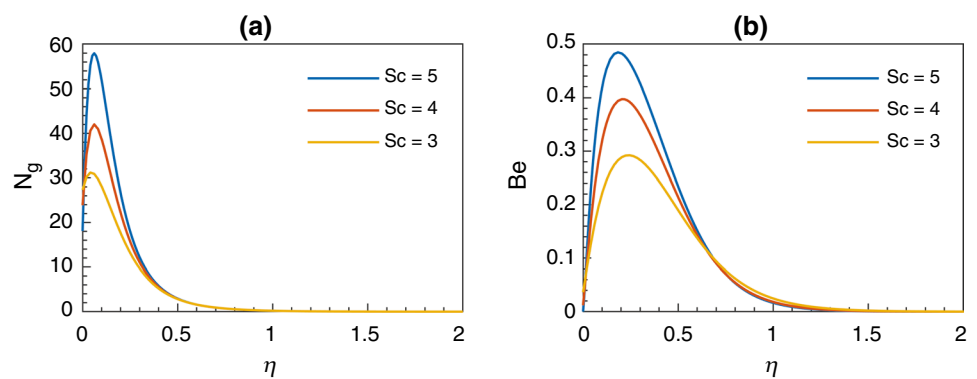
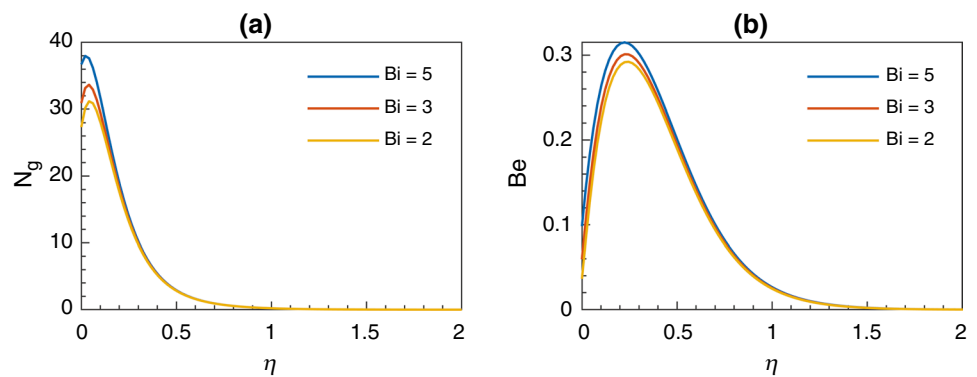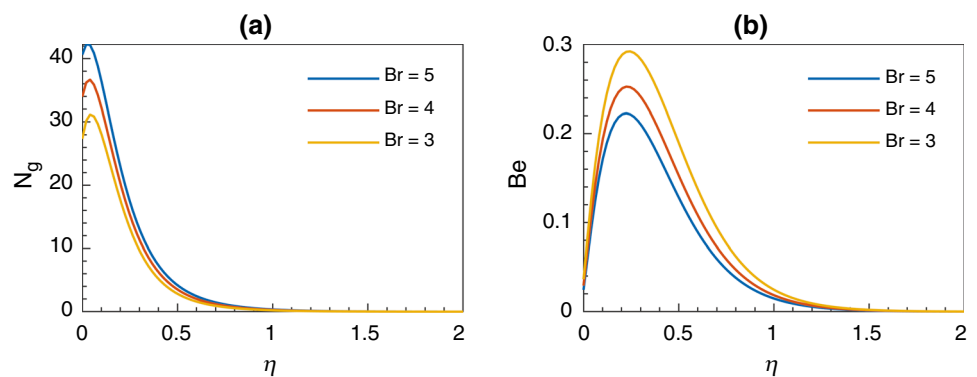Fig. 8 The impact of Biot number on N_g and Be

Fig. 9 The impact of Brinkmann number on N_g and Be

conduction. In contrast to heat transfer irreversibility, fluid flow irreversibility (associated with viscous dissipation) becomes less significant as the Brinkman number decreases. As shownin Fig. 9b, this shift in the irreversibility balance causes the Bejan number to increase overall, indicating that heat transfer is becoming more significant, while remaining below 0.5. A higher temperature difference parameter guides to a reduction in the entropy rate by promoting more effective heat transmission, minimizing temperature variations, and minimizing viscous dissipation. Figure 10a demonstrates that this impact aligns with the notion of minimizing entropy generation in thermodynamic processes wherever possible. As shown in Fig. 10b, as the temperature difference parameter increases, so does the intensity of irreversible

heat transfer, which results in a rise in the Bejan number. Nevertheless, the Bejan number remains below 0.5, suggesting that the irreversibility of fluid flow continues to have a significant impact on the overall irreversibility balance. When the concentration difference parameter is increased, the system encounters a greater concentration gradient, resulting in a stronger driving force for mass transfer. As shown in Fig. 11a, this enhanced efficacy in mass transfer processes contributes to a decline in irreversibilities and, consequently, a reduction in entropy generation. The intensity of mass transfer irreversibilities increases as the concentration difference parameter increases, resulting in an accompanying increase in the Bejan number. As shown in Fig. 11b, the Bejan number remains below 0.5, indicating

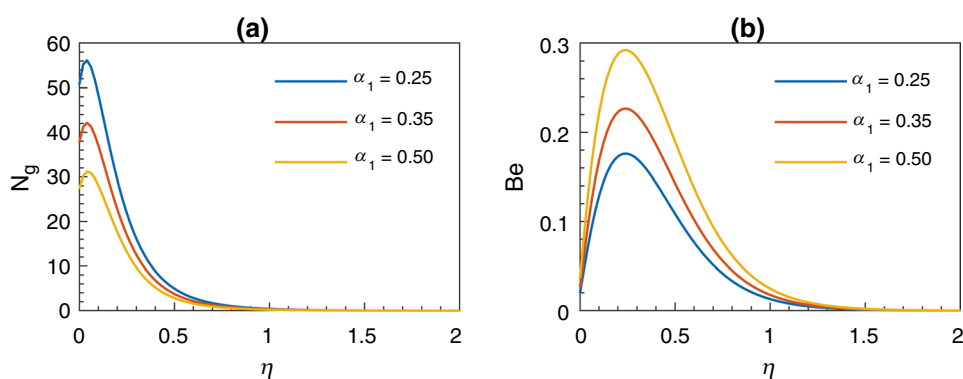**Fig. 10** The impact of temperature difference parameter on N_g and Be

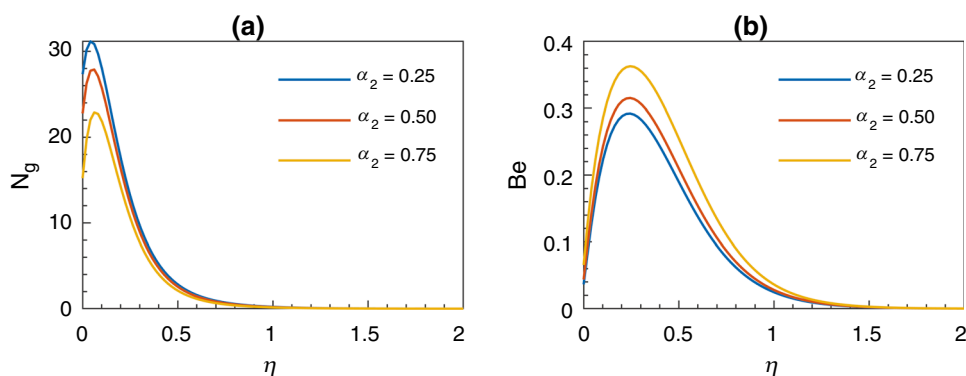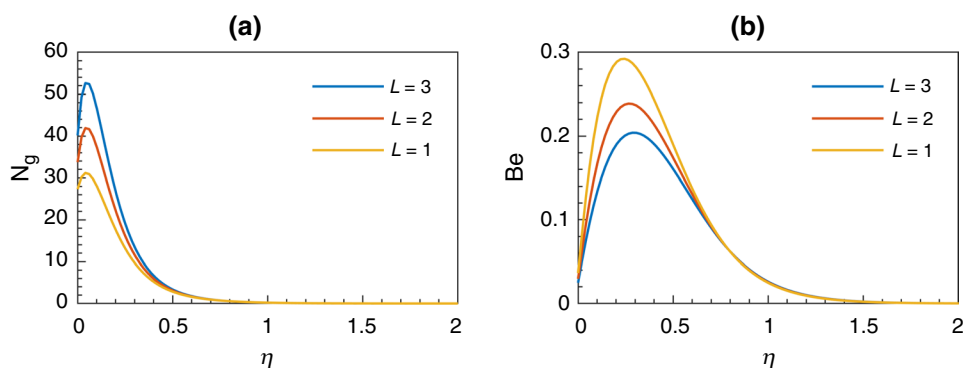**Fig. 11** The impact of concentration difference parameter on N_g and Be

Fig. 12 The impact of diffusive variable on N_g and Be

that the irreversibility of fluid flow continues to contribute considerably to the overall irreversibility balance. As shown in Fig. 12a, a reduction in the parameter representing the diffusive variable signifies a decrease in the generation of entropy that is linked to heat transfer within the system with an inverse impact on Bejan number as shown in Fig. 12b.

Conclusions

This study investigated the intricate dynamics that govern the generation of entropy in heat transfer systems when polymers and nanoparticles are present. We investigated the influence of fluid characteristics on entropy reduction, namely the retardation and extensibility parameters. The FENE-P fluid model provides valuable insights into the optimization of thermodynamic processes by manipulating these parameters. We also observed that polymer concentration significantly reduces the overall entropy of the system. Regarding the Bejan number, a decrease in the diffusive variable parameter resulted in a higher Bejan number, emphasizing the dominance of fluid flow irreversibilities. Remarkably, this dominance was attained while observing the Bejan number below 0.5, emphasizing the delicate balance between heat transmission and fluid flow. The influence of various fluid parameters, including the Dufour number, Soret number, Schmidt number, Biot number, and Brinkman number, on the rate of entropy generation was also thoroughly examined. These observations shed light on our investigation of thermodynamics and fluid dynamics by illuminating the intricate interrelationships that govern the generation of entropy. This understanding provides opportunities for enhancing heat transfer systems, thereby facilitating the development of more efficient and sustainable technology.

Further investigation into this matter might involve exploring alternative models of polymeric fluid in order to complete our understanding of the subject. The primary emphasis of this paper has been on similar analysis; nevertheless, it is possible to expand the scope of this investigation to include non-similar analysis.

References

1. Bejan A. A study of entropy generation in fundamental convective heat transfer, 1979.
2. Bejan A. Second-law analysis in heat transfer and thermal design. In: Advances in heat transfer, vol. 15, Elsevier, 1982, pp. 1–58.
3. Bejan A. Entropy generation minimization: the new thermodynamics of finite-size devices and finite-time processes. J Appl Phys. 1996;79(3):1191–218.
4. Das S, Choi S, Patel H. Heat transfer in nanofluids—a review. Heat Transfer Eng. 2006;27:3–19.
5. Barletta A, Rossi di Schio E, Celli M. Convection and instability phenomena in nano-fluid-saturated porous media. Heat Transfer Enhancement with Nanofluids. Boca Raton: CRC Press; 2015. p. 341–64.
6. Shib Sankar Giri KD, Kundu PK. Heat conduction and mass transfer in a mhd nanofluid flow subject to generalized fourier and fick's law. Mech Adv Mater Struct. 2020;27(20):1765–1775.
7. Rossi di Schio E, Impiombato AN, Mokhefi A, Biserni C. Theoretical and numerical study on buongiorno's model with a couette flow of a nanofluid in a channel with an embedded cavity. Appl Sci. 2022;12(15).
8. Das K, Giri SS, Kundu PK. Influence of hall current effect on hybrid nanofluid flow over a slender stretching sheet with zero nanoparticle flux. Heat Transfer. 2021;50(7):7232–50.
9. Giri SS, Das K, Kundu PK. Stefan blowing effects on MHD bioconvection flow of a nanofluid in the presence of gyrotactic microorganisms with active and passive nanoparticles flux. Eur Phys J. 2017;132:101.
10. Ul-Haq S, Ashraf MB. Entropy analysis in MHD convective flow of carreau fluid over a curved stretching surface with soret and dufour effects. Numer Heat Trans A Appl. 2023;1–20.
11. Asad S, Riaz S. Analysis of entropy generation and nonlinear convection on unsteady flow of MHD Prandtl fluid with Soret and Dufour effects. Arabian J Math. 2023;12(1):49–69.
12. Patil MB, Shobha K, Bhattacharyya S, Said Z. Soret and Dufour effects in the flow of Casson nanofluid in a vertical channel with thermal radiation: entropy analysis. J Therm Anal Calorim. 2023;148(7):2857–67.
13. Khan SA, Hayat T, Razaq A, Momani S. Entropy optimized flow subject to variable fluid characteristics and convective conditions. Alex Eng J. 2024;86:616–30.
14. Ibrahim W, Gizewu T. Analysis of entropy generation of bioconvective on curved stretching surface with gyrotactic microorganisms and third order slip flow. Int J Thermofluids. 2023;17: 100277.
15. Venkateswarlu B, Chavan S, Joo SW, Kim SC. Entropy analysis of electromagnetic trihybrid nanofluid flow with temperature-dependent viscosity in a Darcy-Forchheimer porous medium over a stretching sheet under convective conditions. J Mol Liq. 2024;393: 123660.
16. Hayat T, Razaq A, Khan SA, Momani S. Soret and Dufour impacts in entropy optimized mixed convective flow. Int Commun Heat Mass Transfer. 2023;141: 106575.
17. Khan M, Salahuddin T, Awais M, Altanji M, Ayub S, Khan Q. Calculating the entropy generation of a Bingham plastic fluid flow due to a heated rotating disk. Int Commun Heat Mass Transfer. 2023;143: 106721.

18. Sciacovelli A, Verda V, Sciubba E. Entropy generation analysis as a design tool-a review. Renew Sustain Energy Rev. 2015;43:1167–81.

19. Jameel M, Shah Z, Rooman M, Alshehri MH, Vrinceanu N. Entropy generation analysis on Darcy-Forchheimer Maxwell nanofluid flow past a porous stretching sheet with threshold non-fourier heat flux model and joule heating. Case Studies in Thermal Engineering. 2023;52: 103738.

20. Mandal G, Pal D. Entropy generation analysis of radiated magnetohydrodynamic flow of carbon nanotubes nanofluids with variable conductivity and diffusivity subjected to chemical reaction. J Nanofluids. 2021;10(4):491–505.

21. Rooman M, Jan MA, Shah Z, Alzahrani MR. Entropy generation and nonlinear thermal radiation analysis on axisymmetric mhd ellis nanofluid over a horizontally permeable stretching cylinder. Waves Random Complex Med. 2022;1–15.

22. Boujelbene M, Rehman S, Alqahtani S, Eldin SM, et al. Optimizing thermal characteristics and entropy degradation with the role of nanofluid flow configuration through an inclined channel. Alex Eng J. 2023;69:85–107.

23. Eid MR, Mabood F. Entropy analysis of a hydromagnetic micropolar dusty carbon NTS-kerosene nanofluid with heat generation: Darcy-Forchheimer scheme. J Therm Anal Calorim. 2021;143(3):2419–36.

24. Peterlin A. Hydrodynamics of macromolecules in a velocity field with longitudinal gradient. J Polym Sci C Polym Lett. 1966;4(4):287–91.

25. Bird RB, Dotson PJ, Johnson N. Polymer solution rheology based on a finitely extensible bead-spring chain model. J Nonnewton Fluid Mech. 1980;7(2–3):213–35.

26. Gbadamosi A, Junin R, Manan M, Yekeen NAA. Recent advances and prospects in polymeric nanofluids application for enhanced oil recovery. J Indus Eng Chem. 2018;66:1–19.

27. Olagunju DO. A self-similar solution for forced convection boundary layer flow of a Fene-p fluid. Appl Math Lett. 2006;19(5):432–6.

28. Olagunju DO. Local similarity solutions for boundary layer flow of a FENE-P fluid. Appl Math Comput. 2006;173(1):593–602.

29. Bataller RC. Similarity solutions for boundary layer flow and heat transfer of a FENE-P fluid with thermal radiation. Phys Lett A. 2008;372(14):2431–9.

30. Olagunju DO. The Falkner-Skan flow of a viscoelastic fluid. Int J Non-Linear Mech. 2006;41(6–7):825–9.

31. Anabtawi M, Khuri S. On the generalized Falkner-Skan equation governing boundary layer flow of a FENE-P fluid. Appl Math Lett. 2007;20(12):1211–5.

32. Ahmad A, Ishaq A, Khan Y. Influence of FENE-P fluid on drag reduction and heat transfer past a magnetized surface. Int J Mod Phys B. 2022;36(23):2250145.

33. Khan R, Ahmad A, Afraz M, Khan Y. Flow and heat transfer analysis of polymeric fluid in the presence of nanoparticles and microorganisms. J Central South Univ. 2023;30(4):1246–61.

34. Khan R, Ahmad A. Influence of nanoparticles on the electromagnetic hydrodynamic mixed convection flow and heat transfer of a polymeric fene-p fluid past a riga plate in the presence of arrhenius chemical reaction. J Magn Magn Mater. 2023;567: 170352.

35. Khan R, Ahmad A, Nawaz R. Effects of polymer and dust particles inclusion on drag and heat transfer characteristics in non-newtonian dusty fluids. Numer Heat Trans A Appl. 2023;1–17.

36. Maqbool K, Sohail A, Manzoor N, Ellahi R. Hall effect on Falkner-Skan boundary layer flow of FENE-P fluid over a stretching sheet. Commun Theor Phys. 2016;66(5):547.

37. Khezzar L, Filali A, AlShehhi M. Flow and heat transfer of FENE-P fluids in ducts of various shapes: effect of Newtonian solvent contribution. J Nonnewton Fluid Mech. 2014;207:7–20.

38. Khambhampati KT, Rajagopal K. The derivation of the FENE-P model within the context of a thermodynamic perspective for bodies with evolving natural configurations. Int J Non-Linear Mech. 2021;134: 103729.

39. Vincenzi D, Perlekar P, Biferale L, Toschi F. Impact of the Peterlin approximation on polymer dynamics in turbulent flows. Phys Rev E. 2015;92(5): 053004.

40. Nield D, Kuznetsov A. The Cheng-Minkowycz problem for natural convective boundary-layer flow in a porous medium saturated by a nanofluid. Int J Heat Mass Transf. 2009;52(25–26):5792–5.

41. Khan R, Zaydan M, Wakif A, Ahmed B, Monaledi R, Animasaun IL, Ahmad, A. A note on the similar and non-similar solutions of powell-eyring fluid flow model and heat transfer over a horizontal stretchable surface. In: Defect and Diffusion Forum, vol. 401, Trans Tech Publ, 2020, pp. 25–35.

42. Moore D. A sixth-order extension to the matlab package bvp4c of j. kierzenka and l. shampine (2008).

43. Shampine LF, Kierzenka J, Reichelt MW, et al. Solving boundary value problems for ordinary differential equations in Matlab with bvp4c. Tutorial Notes. 2000;2000:1–27.

44. Cash J, Singhal A. High order methods for the numerical solution of two-point boundary value problems. BIT Numer Math. 1982;22(2):183–99.

45. Cash J, Moore D. High-order interpolants for solutionsof two-point boundary value problems using mirk methods. Comput Math Appl. 2004;48(10–11):1749–63.

46. Cortell R. Viscous flow and heat transfer over a nonlinearly stretching sheet. Appl Math Comput. 2007;184(2):864–73.

47. Vajravelu K. Viscous flow over a nonlinearly stretching sheet. Appl Math Comput. 2001;124(3):281–8.

48. Ramya D, Raju RS, Rao JA, Chamkha A. Effects of velocity and thermal wall slip on magnetohydrodynamics (MHD) boundary layer viscous flow and heat transfer of a nanofluid over a non-linearly-stretching sheet: a numerical study. Propuls Power Res. 2018;7(2):182–95.

49. Bhatnagar R, Gupta G, Rajagopal K. Flow of an Oldroyd-b fluid due to a stretching sheet in the presence of a free stream velocity. Int J Non-Linear Mech. 1995;30(3):391–405.